Optimized Active Power Dispatching of Wind Farms Considering Data-Driven Fatigue Load Suppression

Qi Yao, *Member, IEEE*, Bo Ma, Tianyang Zhao, *Senior Member, IEEE*, Yang Hu, *Member, IEEE*, and Fang Fang, *Senior Member, IEEE*

***Abstract*—The active power fluctuation of wind turbines is not only related to their friendliness to the grid, but also to their fatigue damage. In this paper, the active power of wind turbines in wind farms is optimally scheduled to achieve the suppression of fatigue load of wind turbines. Considering the complexity of fatigue load calculation, it is difficult to apply to real-time active scheduling using metrics that directly characterize fatigue load. To address this problem, a data-driven modeling method for wind turbine fatigue based on deep neural network (DNN) is proposed in this paper, and the relationship between wind speed, power and other easily measurable parameters and fatigue load is established. Further, an improved multi-objective grey wolf optimizer (MOGWO) is designed to achieve the wind farm active scheduling process with the data-driven fatigue calculation results as the optimization objective. The results show that: The fatigue load prediction model of data-driven fatigue calculation proposed in this paper has a satisfactory effect, and the fatigue load of wind turbines can be effectively reduced by adjusting the active power.**

***Index Terms*—Wind turbine, fatigue load, deep neural network, data-driven, multi-objective grey wolf optimizer.**

NOMENCLATURE

DEL	Damage equivalent load
DNN	Deep neural network
MOGWO	Multi-objective grey wolf optimizer
MAE	Mean absolute error
RMSE	Root means square error
WT	Wind turbine
WF	Wind farm
J_{m}	Rotor moment of inertia (Kg/m^3)
J_{e}	Generator moment of inertia (Kg/m^3)
T_{m}	Mechanical torque (N·m)
T_{e}	Generator torque (N·m)
T_{s}	Main shaft torque (N·m)
K_{sp}	Main shaft elastic coefficient (N·m/rad)
K_{vi}	Main shaft damping coefficient (N·m/rad)
ψ	Torsion angle (°)
N_{gaer}	Gear ratio of the gearbox
ω_{r}	Rotor speed (rad/s)
ω_{e}	Generator speed (rad/s)
F_{t}	Aerodynamic thrust (N)
h	Height of the tower (m)
M_{t}	Tower base bending moment (N·m)
v	Wind speed(m/s)
λ	Tip-speed ratio
β	Pitch angle (°)
C_{t}	Thrust coefficient
ρ	Air density (Kg/m^3)
R	Radius of the blade(m)
σ	Stress amplitude
n_j	Number of cycles of the amplitude σ_j
M	Total number of σ_j
ε	Weight coefficients of DNN
b	Bias vectors of DNN
${\chi^l}_i$	Input of the *i-th* neuron in layer *l*
${\varphi^l}_i$	Output of the *i-th* neuron in layer *l*
$N_{l\text{-}1}$	Number of neurons in layer *l-1*
Φ	Activation function of the DNN
$\boldsymbol{Y}$	Vector of the output variable of the DNN.
ζ^l	Partial derivative of the loss function of layer *l*
$P_{\mathrm{e},i}$	Active power of the *i-th* WT
DEL_{Ts}	Drivetrain DEL
DEL_{Mt}	Tower DEL
P_{wf}	Output power of WF
${P^{\min}}_{e,i}$	Minimum power of the *i-th* WT
${P^{\max}}_{e,i}$	Maximum power of the *i-th* WT
η_i	Weighting coefficient in objective function
γ	Penalty coefficient in objective function
Ini	Initial population
Lo^k	Logistic map at the *k* iteration.
Ch^k	Chebyshev map at the *k* iteration

Manuscript received 7 April 2022; revised 15 August 2022; accepted 20 September 2022. Date of publication 12 October 2022; date of current version 19 December 2022. This work was supported in part by the Joint Laboratory of Offshore Wind Power and Intelligent Energy System under Grant HNKJ20-H88-5, in part by the Open Fund of State Key Laboratory of Operation and Control of Renewable Energy and Storage Systems, China Electric Power Research Institute, under Grant NYB51202101982, and in part by the Laboratory of Alternate Electrical Power System with Renewable Energy Sources under Grant LAPS21002. Paper no. TSTE-00351-2022. *(Corresponding author: Bo Ma.)*

Qi Yao, Bo Ma, and Tianyang Zhao are with the Energy and Electricity Research Center, Jinan University, Zhuhai 519070, China (e-mail: yq15811415015@163.com; 1092868529@qq.com; matrixeigs@gmail.com).

Yang Hu and Fang Fang are with the School of Control and Computer Engineering, North China Electric Power University, Beijing 102206, China (e-mail: hooyoung@ncepu.edu.cn; ffang@ncepu.edu.cn).

Color versions of one or more figures in this article are available at https://doi.org/10.1109/TSTE.2022.3213992.

Digital Object Identifier 10.1109/TSTE.2022.3213992

I. INTRODUCTION

IN RECENT years, the installed capacity of wind power generation has been increasing. With the development of wind power, its impact on the grid has become apparent. As a result,

many countries such as Denmark [1] have placed additional requirements on the grid connection of wind power, such as the need for WFs to have the ability to track the active power commands of the grid [2], [3]. However, this will increase the fatigue damage of WTs and have an impact on the economics of WF operation.

Unlike thermal power generation, wind power generation does not cost fuel, so the maintenance cost is one of the most critical factors of concern for operators [4]. Some researchers have chosen to start with the fatigue load of WTs since reducing fatigue loading leads to less damage, which is an important means of reducing maintenance costs [5], [6]. In research and engineering applications, the standard deviation of stress [7], [8] and the damage equivalent load (DEL) [2], [9] are widely recognized as the typical WT fatigue indicators. However, the standard deviation of the stress cannot fully characterize the fatigue load [10]. In contrast, the use of the rain flow counting method [11] and the Palmgren-Miner [12] method to calculate the DEL allows for a more accurate assessment of fatigue. However, due to the complexity of the calculation method, DEL is generally only used for post-assessment of fatigue loads [8].

If a simpler and more effective method for calculating DEL could be available, it would be of great help for online optimization of load suppression. To achieve this goal, Zhang et al. [13] produced a table with wind speed and power as input and DEL as output, and estimated DEL by a look-up table. However, further research shows that there are many parameters that affect the DEL, such as rotor speed, pitch angle, etc. The above table look-up method is too simplified. For such a multi-parameter system, the machine learning algorithm is more effective. The machine learning represented by the deep neural network (DNN) has good performance in data prediction and data fitting [14], [15]. However, there is no research on DEL modeling based on machine learning.

The DEL estimates obtained by machine learning avoid complex mechanism calculations and can be quickly calculated and used to suppress fatigue loads on WTs online. However, a WF usually has dozens of turbines and multi-objective optimization is complex. There are many optimization algorithms similar to Non-dominated sorting genetic (NSGA-II) [16], multi-objective particle swarm optimizer (MOPSO) [17], [18], multi-objective bat (MOBA) [19], multi-objective differential evolution (MODE) [20], multi-objective grey wolf optimizer(MOGWO) [21], [22], etc. To solving multi-objective nonlinear optimization problem. Wang et al. [23] applied the MOGWO to wind speed prediction and compared it with the MOPSO and multi-objective water cycle algorithm (MOWCA). The results showed that the optimization effect of MOGWO is better. Yang et al. [24] proposed that the MOGWO has the advantages of easy implementation and fast convergence. Lu et al. [25] proposed that MOGWO has the disadvantage of low diversity.

Based on the above research status, a data-driven coordinated fatigue suppression model for multiple WTs is studied in this paper to reasonably allocate the active power of WFs, so as to achieve fatigue suppression of the whole WF. The main innovation points are as follows:

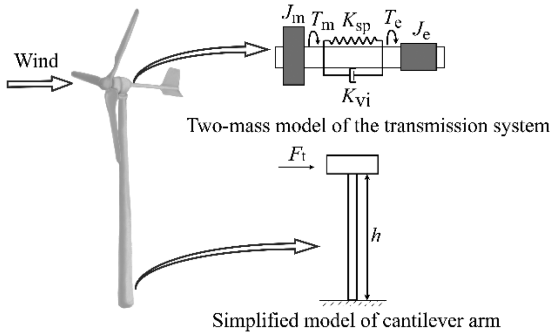

Fig. 1. The causes for the fatigue load of the drivetrain and tower.

1) Machine learning modeling of DEL is implemented. A DNN is designed to calculate DEL using easily measurable parameters such as wind speed, power, rotor speed, and pitch angle as inputs to achieve fast and accurate estimation of DEL.
2) Improved power scheduling algorithm for WFs. MOGWO was improved, and the improved algorithm is used to achieve optimal scheduling, suppressing the fatigue load of the whole WF and reducing the negative optimization of WTs.

This paper is organized as follows. In Section II, the mechanism model of the fatigue load is introduced. In Section III, a DNN for fatigue load modeling is proposed. In Section IV, an improved MOGWO is used for optimization and real-time scheduling. In Section V, the effectiveness of the proposed method is verified. Section VI is the Conclusion.

II. Fatigue Analysis and Modeling of WT

Many mechanical structures of WTs are subjected to fatigue under the action of external loads. In this section, the mechanism of structural fatigue of WT is analyzed and the calculation method of DEL is introduced.

A. Fatigue Analysis of the WT

Due to the complex structure of WTs, fatigue load analysis generally focuses on the main structure. According to the results of [13], the drivetrain is one of the failure-prone structures and has a greater impact on the WT which has a greater impact on the WT. And the damage of the tower will bring the most serious economic loss. Therefore, in this paper, the fatigue loads of the drivetrain and tower are selected for analysis and modeling. The model schematic of the transmission system and the tower is shown in Fig. 1.

1) Drivetrain: The drivetrain can usually be simplified to the two-mass model shown in Fig. 1. The unbalanced torque on both sides is the cause of the fatigue load. The characteristics of the drivetrain can be expressed as follow:

$$\begin{cases} J_{\mathrm{m}}\dot{\omega}_{\mathrm{r}} = T_{\mathrm{m}} - T_{\mathrm{s}} \\ T_{\mathrm{s}} = K_{\mathrm{sp}}\psi + K_{\mathrm{vi}}\dot{\psi} \\ J_{\mathrm{e}}\dot{\omega}_{\mathrm{e}} = T_{\mathrm{s}}/N_{\mathrm{gear}} - T_{\mathrm{e}} \\ \dot{\psi} = \omega_{\mathrm{r}} - \omega_{\mathrm{e}}/N_{\mathrm{gear}} \end{cases} \tag{1}$$

2) Tower: The main source of tower damage is the aerodynamic thrust F_{t} driving the rotation of the turbine, which is related to the wind speed v, pitch angle β, and tip-speed ratio λ. Since the mechanism of the tower is similar to the cantilever arm shown in Fig. 1, researchers usually consider the fatigue load of the tower base as the fatigue load of the whole tower and use the tower base bending moment to evaluate the fatigue load of the tower. The expressions for the force and bending moment of the tower base are shown in (2) and (3).

$$\begin{cases} F_{\mathrm{t}} = 0.5\pi\rho R^2 C_{\mathrm{t}}(\lambda,\beta)v^2 \\ \lambda = \omega_{\mathrm{r}} R/v \end{cases} \tag{2}$$

$$M_{\mathrm{t}} = F_{\mathrm{t}} \cdot h \tag{3}$$

B. DEL Calculation Method

DEL is defined as the amplitude of a sinusoidal stress that produces the same damage as the original signal at a constant frequency f for a time T and is calculated as follows:

$$DEL = \left(\sum_{j=1}^{M} \frac{\sigma_j^m n_j}{Tf} \right)^{\frac{1}{m}} \tag{4}$$

In terms of parameter selection, $Tf = 1$, and $m = 4$.

Based on the definition in (4), the calculation of DEL requires specific information about the original signal. It is necessary to convert the complex load history into a load reversal set that affects fatigue based on the rain flow counting method. And calculate DEL based on the Palmgren-Miner method [26].

In the DEL calculation of WT mechanical structures, DEL can be calculated based on bending moments rather than stresses because the main shaft, tower, etc. can be simplified to a bending uniform section, that is, the fluctuations of T_{s} and M_{t} can be used to calculate the DEL [27].

According to (4), the calculation of DEL depends on the accurate measurement of T_{s} and M_{t}. And the calculation process of rain flow counting is complicated. These conditions make it difficult to apply DEL to the online control of WTs.

III. Deep Neural Network For DEL Calculation

Based on Section II, the mechanism calculation method of DEL is relatively complicated and difficult to be applied to the online control of WTs. This section attempts to realize the fast calculation of DEL by constructing a DNN.

A. Parameter Selection For DNN

In order to use a DNN to calculate DEL, this subsection begins by selecting the parameters related to DEL as the input to the DNN. The input should be easily measurable, not conventional torque data. According to (1)–(4), the easily measurable parameters related to DEL of the drivetrain and tower include wind speed, rotor speed, pitch angle and active power. Therefore, this section constructs the input of DNN based on the above parameters as shown in Table I.

According to the definition of DEL, the magnitude and fluctuation of pressure are two important dimensions that affect DEL.

TABLE I
Nine Selected Indicators for the Input of DNN

Related parameter	Selected indicator	Mathematical expression
Wind speed	Mean of wind speed	$\overline{v} = \frac{1}{N_2}\sum_{i=1}^{N_2} v_i$
	Turbulence Intensity	$I = \frac{1}{\overline{v}}\sqrt{\sum_{i=1}^{N_2}(v_i - \overline{v})^2/(N_2-1)}$
Active power	Mean of power	$\overline{P}_{\mathrm{e}} = \frac{1}{N_2}\sum_{i=1}^{N_2} P_{ei}$
	Standard deviation of power	$\mathrm{std}(P_{\mathrm{e}}) = \sqrt{\sum_{i=1}^{N_2}(P_{ei} - \overline{P}_{\mathrm{e}})^2/(N_2-1)}$
	Standard deviation of power fluctuation	$\mathrm{std}(\Delta P_{\mathrm{e}}) = \sqrt{\sum_{i=1}^{N_2}(\Delta P_{ei} - \Delta\overline{P}_{\mathrm{e}})^2/(N_2-1)}$
Pitch angel	Mean of pitch angle	$\overline{\beta} = \frac{1}{N_2}\sum_{i=1}^{N_2} \beta_i$
	Standard deviation of pitch angle	$\mathrm{std}(\beta) = \sqrt{\sum_{i=1}^{N_2}(\beta_i - \overline{\beta})^2/(N_2-1)}$
Rotor speed	Mean of rotor speed	$\overline{\omega}_{\mathrm{r}} = \frac{1}{N_2}\sum_{i=1}^{N_2} \omega_{ri}$
	Standard deviation of rotor speed	$\mathrm{std}(\omega_{\mathrm{r}}) = \sqrt{\sum_{i=1}^{N_2}(\omega_{ri} - \overline{\omega}_{\mathrm{r}})^2/(N_2-1)}$

TABLE II
NREL 5MW WT Parameters

Parameter	Theoretical value
Cut-in wind speed, rated wind speed, cut-out wind speed	3m/s, 11.4m/s, 25m/s
The diameter of the rotor disc	126m
rated power	5MW
Starting speed, rated speed	6.9rpm, 12.1rpm

Therefore, the metrics constructed in this paper are in the form of mean and standard deviation. In practical application, the above nine indicators can be obtained from the data in the SCADA system by simple calculation, which is easier to obtain compared to torque.

B. Data Preparation For DNN

In order to characterize the coupling between the above parameters and DEL, a Monte Carlo experiment based on SimWindFarm [28] is designed in this subsection to generate the operational data. The experiment was conducted on a simulated WT, the NREL 5MW, which is widely used in research in this field and developed by the National Renewable Energy Laboratory. Parameters such as wind speed and power have been artificially designed in order to simulate different working conditions. The WT parameters and experimental parameters are set as shown in Tables II and III.

In Table I, the mean of wind speed, turbulence intensity, and mean of power are preset by SimWindFarm. A total of 480 sets of working conditions are set at equal intervals. The standard deviation of power and power fluctuations cannot be preset. In this paper, a range of variable random numbers are added to the power set values in the simulation, and there are a total of 100

TABLE III
SETTING OF EXPERIMENTAL CONDITIONS FOR WTS

parameter	Working condition	Interval
Average wind speed	6 - 20m/s	2 m/s
Turbulence intensity	0.1 - 0.2	0.02
Average power	0.5 – 5MW	0.5 MW
Power random number	0.01 – 1MW	0.01 MW

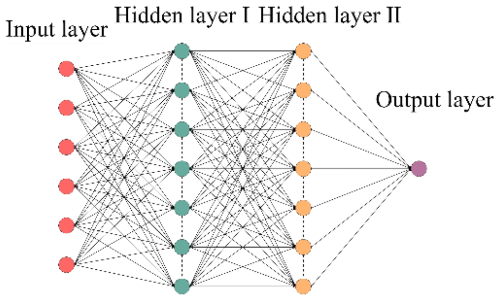

Fig. 2. Schematic diagram of DNN.

sets of random numbers. Therefore, 48000 different working conditions were constructed for the experiments in this paper. A total of 48000 sets of data were obtained for training DNN. In the acquisition of experimental data, each group of data is calculated for 300 s with a sampling interval of 1 s. That is, the mean, variance and other parameters are found for the data of 300 time points.

The above nine indicators are obtained from the equations in Table I. DEL_{Ts} and DEL_{Mt} are calculated by the MCrunch code [26]. DEL is also calculated as the other parameters mentioned before, using the data sampled over 300 s to obtain. After data collection, the Pearson correlation coefficient (PCC) are shown in Table IV.

The numbers in Table IV indicate the correlation between the data. The higher the number, the higher the correlation. Negative (positive) numbers indicate negative (positive) correlation [30]. In this paper, the six sets of data with the highest correlation with DEL_{Ts} and DEL_{Mt} are selected as input, $\mathrm{DEL}_{\mathrm{Ts}}$ and DEL_{Mt} as output for DNN training. Six sets of data with higher correlation with DEL_{Ts} are I, $\bar{P}_{\mathrm{e}}$, $\mathrm{std}(P_{\mathrm{e}})$, $\mathrm{std}(\Delta P_{\mathrm{e}})$, $\mathrm{std}(\beta)$ and $\mathrm{std}(\omega_{\mathrm{r}})$. Six sets of data with higher correlation with DEL_{Mt} are I, $\bar{v}$, $\bar{P}_{\mathrm{e}}$, $\mathrm{std}(P_{\mathrm{e}})$, $\mathrm{std}(\Delta P_{\mathrm{e}})$, $\mathrm{std}(\beta)$, $\bar{\omega}_{\mathrm{r}}$.

C. Model Structure of DNN

DNN includes an input layer, several hidden layers and an output layer, as shown in Fig. 2. The first layer is the input layer, the last layer is the output layer, and the middle layers are the hidden layers. All neurons between adjacent layers are interconnected. There are forward transmission and backward transmission in DNN. Forward transmission initially builds a neural network, and backward transmission optimizes the neural network.

1) Forward Transmission: Each two neurons of adjacent layers have different weight coefficients bias ε vectors b between. In (5)–(6), ε and b are used for data transfer from the input layer to the output layer.

$$\chi_i^l = \sum_{j=1}^{N_{l-1}} \varepsilon_{ij}^l \varphi_j^{l-1} + b_i^l \tag{5}$$

$$\varphi_i^l = \Phi(\varepsilon_{ij}^l \varphi_j^{l-1} + b_i^l) \tag{6}$$

2) Back Transmission: The purpose of backpropagation is to complete the update of the weight coefficient ε and the bias vector b in forward propagation by rational iterative optimization of the loss function. The loss function in this paper is defined as follows:

$$J = \frac{1}{2} \left\| \boldsymbol{\varphi}^L - \boldsymbol{Y} \right\|_2^2 \tag{7}$$

To complete the update of the weight coefficient ε and the bias vector b, the following calculations are performed:

$$\varsigma^l = \frac{\partial J}{\partial \chi^L} = (\boldsymbol{\varphi}^L - \boldsymbol{Y}) \otimes \Phi'(\chi^L) \tag{8}$$

$$\frac{\partial J}{\partial \omega^l} = \varsigma^l (\boldsymbol{\varphi}^{L-1})^{\mathrm{T}} \tag{9}$$

$$\frac{\partial J}{\partial b^l} = \varsigma^l \tag{10}$$

where ς^l is the partial derivative of the loss function of layer l.

The updates of ε and b are shown in (9)–(10). However, in the training of the DNN, the parameters may deviate from their set ranges when the depth of the network increases. To solve the problem, the Adam algorithm is used in this paper to calculate the exponentially weighted average of the gradient while training. The obtained gradient values are used to update the parameters. The related algorithm can be found in [31].

Based on the above data and DNN, a fast calculation model for DEL can be obtained, as shown in following formula:

$$DEL_{\mathrm{Ts}} = DNN_{\mathrm{Ts}}(I, \bar{P}_{\mathrm{e}}, \mathrm{std}(P_{\mathrm{e}}), \mathrm{std}(\Delta P_{\mathrm{e}}), \mathrm{std}(\beta), \mathrm{std}(\omega_{\mathrm{r}})) \tag{11}$$

$$DEL_{\mathrm{Mt}} = DNN_{\mathrm{Mt}}(I, \bar{v}, \bar{P}_{\mathrm{e}}, \mathrm{std}(P_{\mathrm{e}}), \mathrm{std}(\Delta P_{\mathrm{e}}),\ \mathrm{std}(\beta), \bar{\omega}_{\mathrm{r}}) \tag{12}$$

IV. ACTIVE POWER DISPATCH OF WFS WITH IMPROVED MOGWO

Based on the data-driven model constructed in Section III, DEL can be quickly calculated using readily available data for real-time fatigue load suppression. Based on the above modeling results, it can be seen that the DEL of the drivetrain and tower strongly related to the active power. Active power is an important target for WF control considering grid friendliness. Therefore, in this paper, the active power output of each WT is treated as a decision variable. Fatigue load reduction is achieved by adjusting the power output of all WTs within the same WF. In this section, the active power distribution with DEL as the optimization objective is mathematically modeled.

TABLE IV
PCC OF DEL AND THE SELECTED INDICATORS

	I	$\overline{v}$	$\overline{P}_e$	std(P_e)	std(ΔP_e)	$\overline{\beta}$	std(β)	$\overline{\omega}_r$	std(ω_r)	DEL_{Ts}	DEL_{Mt}
I	1										
$\overline{v}$	-0.415**	1									
$\overline{P}_e$	-0.223**	0.411**	1								
std(P_e)	0.299**	-0.246**	0.047**	1							
std(ΔP_e)	-0.167**	0.369**	0.101**	0.436**	1						
$\overline{\beta}$	-0.391**	0.957**	0.180**	-0.326**	0.404**	1					
std(β)	0.195**	0.392**	0.465**	0.022**	0.428**	0.349**	1				
$\overline{\omega}_r$	-0.411**	0.747**	0.399**	-0.195**	0.519**	0.757**	0.694**	1			
std(ω_r)	0.602**	-0.560**	-0.091**	0.495**	-0.160**	-0.637**	0.028**	-0.499**	1		
DEL_{Ts}	0.208**	-0.030**	0.114**	0.868**	0.668**	-0.088**	0.153**	-0.029**	0.288**	1	
DEL_{Mt}	0.237**	0.318**	0.522**	0.156**	0.388**	0.234**	0.766**	0.448**	0.037**	0.353**	1

**: Significantly correlated at the 0.01 level (two-sided).

A. Objective Function Settings

The optimization algorithm in this section is used for active power control. Therefore, the power requirements of the WF and the upper and lower limits of each WT need to be satisfied while achieving the objective of fatigue load suppression. Without loss of generality, it can be formulated as a minimization problem as follows:

$$\text{minimize}: \quad \sum_{i=1}^{N_3} DEL_{\mathrm{Ts},i}|P_{\mathrm{e},i} + \sum_{i=1}^{N_3} \eta_i \cdot DEL_{\mathrm{Mt},i}|P_{\mathrm{e},i} \tag{13}$$

$$\text{subject to}: \quad P_{\mathrm{wf}} = \sum_{i=1}^{N_3} P_{\mathrm{e},i} \tag{14}$$

$$P_{\mathrm{e},i}^{\min} \le P_{\mathrm{e},i} \le P_{\mathrm{e},i}^{\max} \tag{15}$$

where $DEL_{\mathrm{Ts},i}|P_{\mathrm{e},i}$ and $DEL_{\mathrm{Mt},i}|P_{\mathrm{e},i}$ are the DEL_{Ts} and DEL_{Mt} when the active power of the *i-th* WT is $P_{\mathrm{e},i}$. The best reference value for each WT is assigned in real time by using the power as a decision variable for DEL seeking, while meeting the grid demand.

To deal with the constraints in (14) in the optimization process, this paper adds it to the objective function as a penalty function by adding a penalty coefficient γ. Thus, the objective function form is changed to the following formula.

$$\min \sum_{i=1}^{N_3} DEL_{\mathrm{Ts},i}|P_{\mathrm{e},i} + \sum_{i=1}^{N_3} \eta_i \cdot DEL_{\mathrm{Mt},i}|P_{\mathrm{e},i} + \gamma \cdot \left| P_{\mathrm{wf}} - \sum_{i=1}^{N_3} P_{\mathrm{e},i} \right| \tag{16}$$

The upper and lower bound constraints in (15) are easy to handle in the optimization algorithm.

In the above model, the WF output power needs to meet the power grid control requirements (e.g., frequency regulation), while minimize the aggregate of DEL of all WTs in the WF, through optimizing the power command value of each WT under different working conditions.

B. Improved MOGWO

The problems mentioned above are non-linear and non-convex. Considering the application effects of multiple optimization algorithms, a MOGWO algorithm [22] is improved and applied in this section. The principle of MOGWO can be found in [22].

1) Optimization of the Initial Population: The improvement of the initial population uniformity is also an important way to improve global convergence, avoid falling into local optimal and reduce negative optimization [32]. The traditional MOGWO uses a random function to generate the initial population, which has poor population uniformity. In this section, the chaotic sequence [33] is used to generate the initial population to improve the diversity and traversal of the population. To obtain better uniformity, this section uses the chaotic sequence obtained by mixing Logistic and Chebyshev. The ratio of the two mappings is set to 0.5.

$$\begin{cases} Ini^{k+1} = 0.5Lo^{k+1} + 0.5\left|Ch^{k+1}\right| \\ Lo^{k+1} = \delta \cdot Lo^{k} \cdot (1 - Lo^{k}) \\ Ch^{k+1} = \cos(2\arccos(Ch^{k})) \end{cases} \tag{17}$$

Where δ is a certain coefficient, the value range is [04].

2) Optimization of the Weight: In optimization, DEL_{Ts} and DEL_{Mt} are not in the same order of magnitude. Therefore, an appropriate weighting factor between them is needed to make the optimization more balanced. The Pareto front is used to optimize the weights in this section. After the Pareto solution set is obtained, the weight coefficients are obtained as follows:

$$\eta_i = \sum_{j=1}^{M} F_{\mathrm{Mt},j}^{i} \Big/ \sum_{j=1}^{M} F_{\mathrm{Ts},j}^{i} \tag{18}$$

$$F_{\mathrm{wt},j}^{i} = F_{\mathrm{Mt},j}^{i} + \eta_i \cdot F_{\mathrm{Ts},j}^{i} \tag{19}$$

where η_i is mentioned in (16), $F_{\mathrm{Mt},j}$ is the *j-th* solution of DEL_{Mt} in the Pareto solution set, $F_{\mathrm{Ts},j}$ is the *j-th* solution of DEL_{Ts} in the Pareto solution set. $F_{\mathrm{wt},j}^{i}$ is the *j-th* solution of the *i-th* WT's DEL. In this paper, the solution with the smallest $F_{\mathrm{wt},j}^{i}$ in the Pareto solution set is taken as the optimal solution.

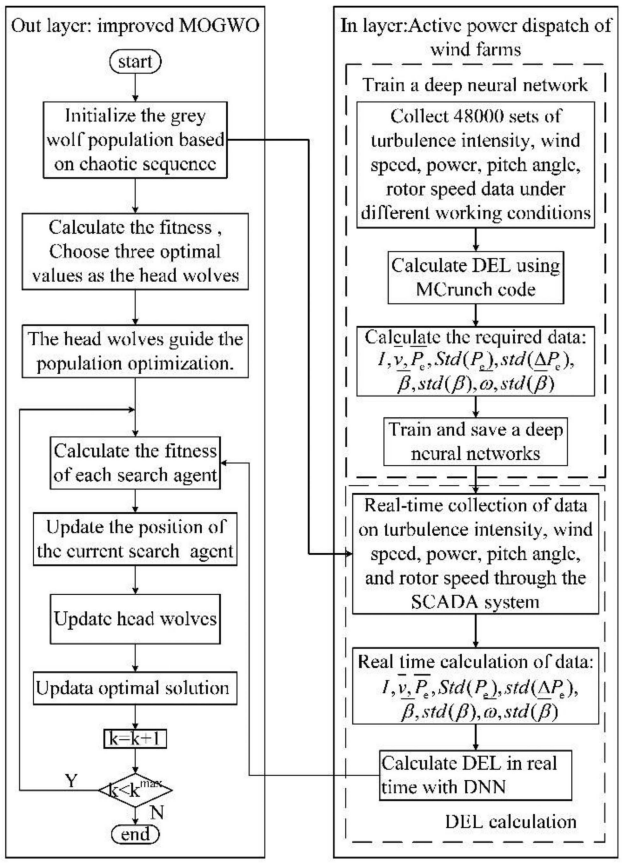

Fig. 3. The optimization framework of the fatigue load suppression.

C. Overall Architecture of the Optimization Algorithm

In this section, the objective function and constraints to suppress fatigue loading are determined. Combined with the data-driven model proposed in Section III, MOGWO is improved. The active control flow chart of fatigue suppression combined with the improved MOGWO is shown in Fig. 3. In the next section, the simulation results of the problem proposed in this paper will be displayed and analyzed.

V. Case Study

A. DNN Training Results

To test the performance of the DNN, this paper divides 48000 groups of different working conditions into 45000 groups and 3000 groups. Among them, the 45000 sets of data are set as the training set, The rest are set as the test set. After getting the data-driven model, root means square error (RMSE) and mean absolute error (MAE) are used to evaluate the performance of the model. In the prediction of DEL_{Ts} and DEL_{Mt}, RMSE are both close to 0, MAE between the predicted result and the actual result are 13.67% and 15.47%. In terms of computational resource usage, a computer with Intel(R) Core (TM) i5-12600K CPU @ 3.70 GHz processor and 32 GB RAM is used. It takes about 12 minutes to train DNN with RMSE at a reasonable level. The predicted data can basically fit the original data, as shown in Figs. 4 and 5.

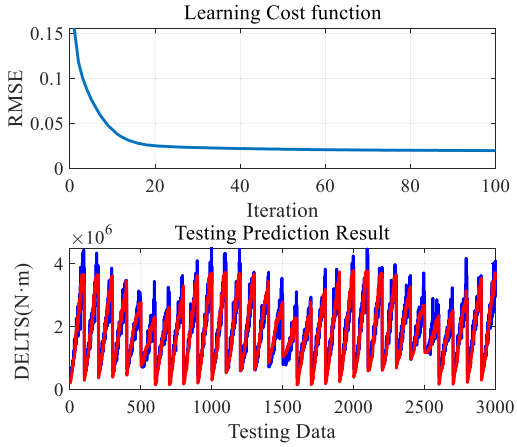

Fig. 4. Performance evaluation of DNN in predicting DEL_{Ts}.

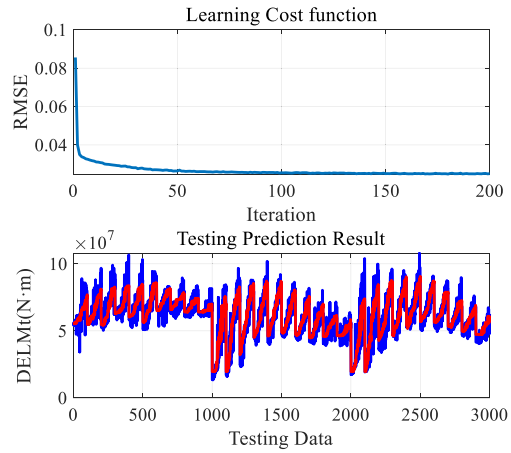

Fig. 5. Performance evaluation of DNN in predicting DEL_{Mt}.

The results show that the data-driven model can be used to calculate the fatigue load of the drivetrain and tower with simple data such as wind speed, power, pitch angle, rotor speed, and so on. Further, to demonstrate the sensitivity of the DNN to the training data, a portion of the work conditions are artificially removed from the training set. By varying the proportion of the training group data to all the working conditions in the dataset, it is demonstrated that the DNN is sensitive to the training data, i.e., when the working conditions of the training data become significantly incomplete, a certain degree of degradation of the model accuracy occurs. The working condition settings and test results are shown in Table V. It can be seen that the reasonable selection of the working conditions used for modeling will be an important direction to improve the accuracy of DEL modeling in future research.

B. Optimal Dispatching Simulation of Active Power

A WF model based on SimWindFarm is built in this case. The simulated WF contains 12 NREL 5 MW WTs, which are arranged in the form of 4 × 3. The distance between each WT is 500 m, as shown in Fig. 6. In the simulation, the wind speed fluctuations are shown in Fig. 7. To verify the effectiveness of

TABLE V
DNN ACCURACY TEST UNDER MISSING TRAINING DATA

parameter	Modeling data scale	Modeling conditions	Testing conditions	MAE (DEL_{Ts})	MAE (DEL_{Mt})
Average wind speed	100%	6-20m/s	6-20m/s	13.67%	15.47%
	80%	6-18m/s	18-20m/s	13.79%	21.15%
	60%	6-14m/s	14-20m/s	14.56%	22.25%
	40%	6-12m/s	12-20m/s	17.83%	26.38%
Average power	100%	0.5-5MW	0.5-5MW	13.67%	15.47%
	80%	0.5-4MW	4.5-5MW	14.53%	18.32%
	60%	0.5-3MW	3.5-5MW	15.32%	20.64%
	40%	0.5-2MW	2.5-5MW	17.69%	24.83%

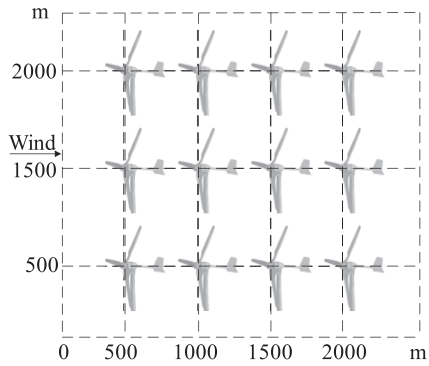

Fig. 6. Schematic layout of the WF.

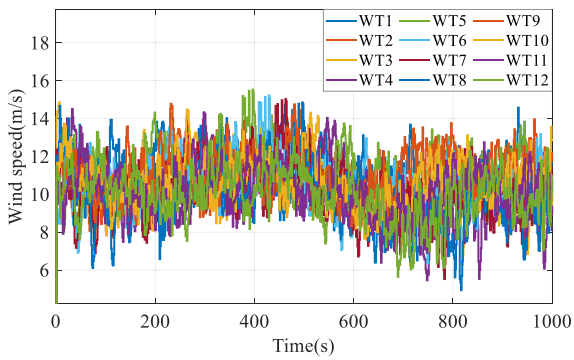

Fig. 7. Simulation wind speed.

the proposed method, the proportional distribution algorithm (PDA) commonly used in engineering [34] and the fatigue load representation method (FLRM) based on the look-up table [13] are used for comparison. Both the FLRM and the proposed method used the improved MOGWO algorithm as the optimization method.

The simulation in this paper verifies the fatigue load optimization effect of WF during constant power and power ramp-up. The power reference value of the WF is set as follows: In the first 400 s, the power reference value is 12 MW. In the 400 s to 700 s, the power linearly climbs to 24 MW. In the last 300 s, the power remained at 24 MW. The WT start-up process exists in the first 100 s of the simulation, which is an unstable operation process, and the algorithm in this paper requires 300 s of continuous stable operation state parameters for the data-driven calculation of DEL. Therefore, the traditional PDA is used for the first 400

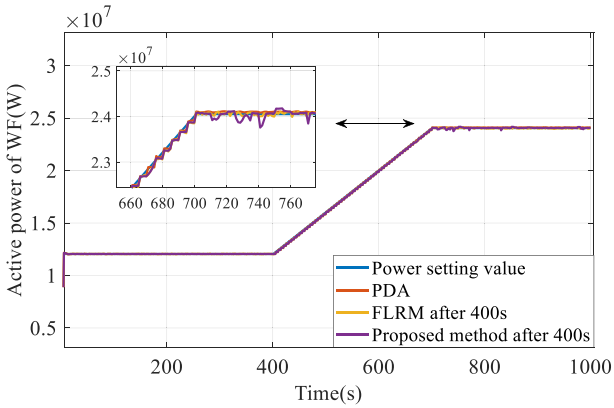

Fig. 8. Comparison of active power control of the WF.

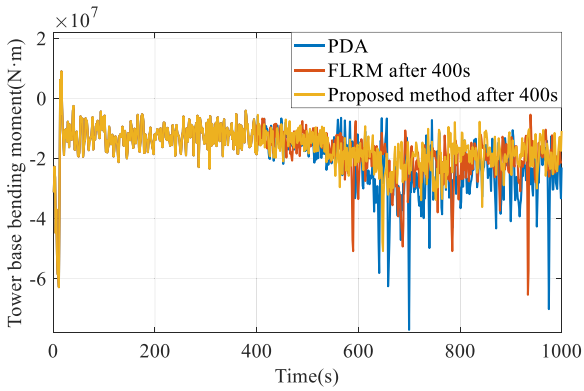

Fig. 9 Comparison of T_s of WT 1#.

s of the simulation, and the comparison of different algorithms is performed in the last 600 s. The power tracking results of the three different algorithms are shown in Fig. 8. Based on the simulation results, the MAE metrics of PDA, FLRM and the proposed method in tracking WF power commands are 0.18%, 0.21% and 0.25%, respectively. It can be seen that the use of the optimized algorithm hardly affects the power tracking effect, and the tracking errors of several methods are acceptable.

Although all three methods can track the commanded value of active power well, there is a big gap between each method in terms of fatigue load suppression. WT 1# was selected as an example to compare the main shaft torque and tower bending moment controlled by the three algorithms, as shown in Figs. 9 and 10. In the last 600 s, three different algorithms were used to control the WT 1#. It can be seen that after the optimization of the proposed algorithm, the fluctuations of the main shaft torque and tower bending moment of WT 1# smoother and the amplitude are reduced, which is a sign of load reduction. To further quantitatively evaluate the optimization effect, MCrunch [26] is used to calculate the accurate DEL of all WTs under the control of the three algorithms. The results are shown in Tables VI, and VII.

From the calculation results in Tables VI and VII, it can be seen that both FLRM and the proposed method reduce the total fatigue of WTs compared to the conventional PDA, due to the fact that both methods take the suppression of DEL into account

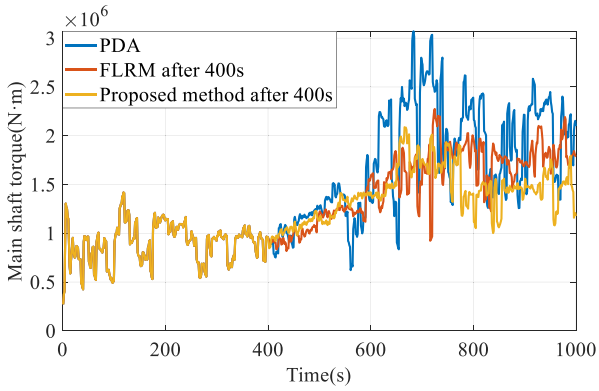

Fig. 10. Comparison of M_t of WT 1#.

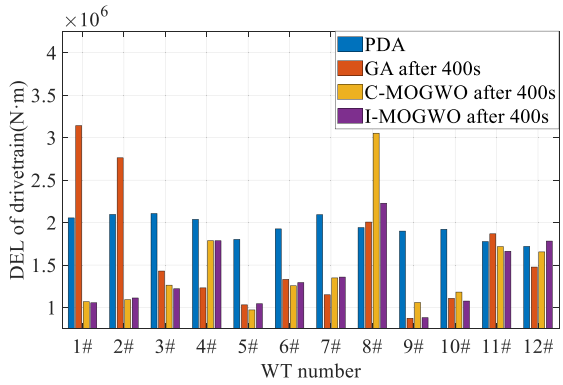

Fig. 11. DEL comparison of the drivetrain of all WTs.

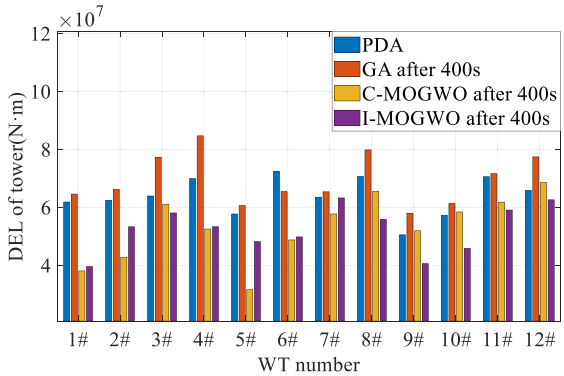

Fig. 12. DEL comparison of the tower of all WTs.

TABLE VI
DEL COMPARISON OF THE DRIVETRAIN (UNIT: MN·M)

WT	PDA	FLRM	Proposed method
1#	2.06	2.14(-4.21%)	1.06(48.63%)
2#	2.10	2.16(-3.34%)	1.11(46.93%)
3#	2.11	1.73(19.96%)	1.22(42.06%)
4#	2.04	1.63(5.24%)	1.79(12.35%)
5#	1.80	1.33(26.13%)	1.04(42.04%)
6#	1.93	1.13(41.25%)	1.29(32.82%)
7#	2.10	1.45(30.74%)	1.36(35.09%)
8#	1.94	2.31(-18.81%)	2.23(-14.78%)
9#	1.90	1.14(39.98%)	0.88(53.64%)
10#	1.92	1.51(21.51%)	1.08(43.98%)
11#	1.78	1.58(11.09%)	1.66(6.43%)
12#	1.72	1.54(10.65%)	1.78(-3.65%)
WF	23.38	19.65(16.08%)	16.50(28.79%)

TABLE VII
DEL COMPARISON OF THE TOWER (UNIT: MN·M)

WT	PDA	FLRM	Proposed method
1#	64.59	61.86(4.24%)	39.59 (38.71%)
2#	66.22	62.45(3.39%)	53.30 (19.50%)
3#	77.31	68.93(10.84%)	58.08 (24.87%)
4#	84.68	73.32(13.41%)	53.33 (37.02%)
5#	60.65	60.73(-0.13%)	48.21 (20.51%)
6#	65.49	58.49(10.69%)	49.81 (23.94%)
7#	65.37	65.52(-0.23%)	63.26 (3.22%)
8#	79.82	56.27(29.50%)	55.90 (29.98%)
9#	58.00	58.35(-0.61%)	40.61 (29.98%)
10#	61.37	58.28(5.04%)	45.86 (25.26%)
11#	71.65	64.60(9.84%)	59.08 (17.53%)
12#	77.42	68.87(11.04%)	62.61 (19.13%)
WF	832.60	766.87(7.42%)	629.67 (24.14%)

during optimization. It can be seen that the goal of fatigue suppression can be achieved even without using an accurate model of WT.

It can also be seen that the optimization of the proposed method in this paper is better than FLRM. This is because the conventional FLRM algorithm only considers the linear coupling between the DEL and the operating parameters of the WTs, and the nonlinear relationship between the parameters is ignored. In contrast, the method in this paper provides a more accurate modeling of the DEL, so that the fatigue of the WT can be more accurately described in the optimization, which can guide the optimization algorithm to find a more optimal solution.

C. Comparison of the Improvement Effect of the Optimization Algorithms

In this section, the effect of different optimization algorithms is compared under the same simulation settings in Section IV.B. The conventional MOGWO (C-MOGWO) and GA are compared with the proposed improved MOGWO (I-MOGWO). The comparison results are shown in Figs. 11 and 12.

Based on the DNN-driven DEL model, the three optimization algorithms all reduce the total fatigue of WTs. For the sum of the DEL of all the WT drivetrains in the WF, the results obtained by the GA, C-MOGWO and I-MOGWO are 19.41 MN·m, 17.46 MN·m and 16.50 MN·m, respectively. For the tower, the results obtained by the three algorithms are 674.69 MN·m, 639.02 MN·m and 629.67 MN·m, respectively. The results show that MOGWO has stronger optimization ability than GA, and the improvement made in this paper further improves the optimization effect.

Further, to verify the stability of the optimization capability of the improved algorithm, 30 independent replicate experiments were conducted for I-MOGWO and C-MOGWO based on the above simulation WF and experimental setup, and the comparison results are shown in Table VIII.

TABLE VIII
OPTIMIZATION EFFECTS OF THE INDEPENDENT REPLICATE EXPERIMENTS

Method	Indicator	Average global optimization rate of WF	Maximum negative optimization ratio of single WT
C-MOGWO	DEL_{Ts}	22.97%	34.01%
	DEL_{Mt}	19.28%	38.33%
I-MOGWO	DEL_{Ts}	24.64%	27.03%
	DEL_{Mt}	20.49%	26.89%

In Table VIII, "Average global optimization rate of WF" indicates the average optimization ratio of DEL_{Ts} and DEL_{Mt} for all WTs compared to PDA during the replicate experiments, and "Maximum negative optimization ratio of single WT" indicates the maximum negative optimization ratio of single WT during the replicate experiments. The results show that I-MOGWO is more effective in suppressing DEL, while the optimization search process leads to less extreme negative optimization of individual WTs. It is of interest to optimize the initial population using chaotic sequences to improve the optimization capability.

VI. CONCLUSION

In this paper, a data-driven model is constructed to calculate the DEL of WTs and applied to active power control of a WF and fatigue load suppression of WTs based on the improved MOGWO.

In the data-driven modeling section, the fatigue load of WTs is modeled based on DNN. Parameters that can be easily measured during WTs operation (e.g., active power, rotor speed, etc.) are used as inputs to the DNN, and the DEL in WT structure is used as output of DNN. After evaluation by MAE, the final WT fatigue fast calculation models with 13% and 15% prediction error for DEL_{Ts} and DEL_{Mt} were obtained. Based on the proposed fast calculation model for DEL, the fatigue load is effectively suppressed in the active power control of a WF based on the improved MOGWO. Compared with PDA, the proposed optimization algorithm helps reduce the total DEL of the WT drivetrain by more than 28%, and the DEL of the tower by more than 24%. Further, the proposed algorithm also exhibits 14.0% and 17.9% advantages over FLRM in terms of DEL suppression for drivetrain and tower due to the advantages brought by accurate modeling of DEL.

The contents studied in this paper can provide a good basis for improving the flexible and economic operation of WFs. In future research, it is planned to improve the data used for modeling to the values obtained from actual measurements, and to investigate the effect of noisy data on model accuracy during real measurements and the problem of model updating on longer time scales, so as to promote the practical use of the proposed algorithm.

REFERENCES

[1] "Regulations for grid connection." Apr. 27, 2019. Accessed: Nov. 21, 2021. [Online]. Available: https://en.energinet.dk:443/Electricity/Rules-and-Regulations/Regulations-for-grid-connection

[2] Q. Yao, Y. Hu, H. Deng, Z. Luo, and J. Liu, "Two-degree-of-freedom active power control of megawatt wind turbine considering fatigue load optimization," *Renewable Energy*, vol. 162, pp. 2096–2112, Dec. 2020.

[3] X. Tang, M. Yin, C. Shen, Y. Xu, Z. Y. Dong, and Y. Zou, "Active power control of wind turbine generators via coordinated rotor speed and pitch angle regulation," *IEEE Trans. Sustain. Energy*, vol. 10, no. 2, pp. 822–832, Apr. 2019.

[4] J. Zhang, Y. Liu, D. Tian, and J. Yan, "Optimal power dispatch in WF based on reduced blade damage and generator losses," *Renewable Sustain. Energy Rev.*, vol. 44, pp. 64–77, Apr. 2015.

[5] C. E. Plumley, W. E. Leithead, P. Jamieson, M. Graham, and E. Bossanyi, "Supplementing wind turbine pitch control with a trailing edge flap smart rotor," in *Proc. IEEE 3rd Renewable Power Gener. Conf.*, 2014, pp. 1–6.

[6] A. D. Wright, L. J. Fingersh, and K. A. Stol, "Testing controls to mitigate fatigue loads in the controls advanced research turbine," in *Proc. IEEE 17th Mediterranean Conf. Control Automat* ., 2009, pp. 1275–1282.

[7] B. Biegel, D. Madjidian, V. Spudic, A. Rantzer, and J. Stoustrup, "Distributed low-complexity controller for wind power plant in derated operation," in *Proc. IEEE Int. Conf. Control Appl* ., 2013, pp. 146–151.

[8] H. Zhao, Q. Wu, Q. Guo, H. Sun, and Y. Xue, "Distributed model predictive control of a wind farm for optimal active power controlpart I: Clustering-based wind turbine model linearization," *IEEE Trans. Sustain. Energy*, vol. 6, no. 3, pp. 831–839, Jul. 2015.

[9] H. Zhao, Q. Wu, S. Huang, M. Shahidehpour, Q. Guo, and H. Sun, "Fatigue load sensitivity-based optimal active power dispatch for wind farms," *IEEE Trans. Sustain. Energy*, vol. 8, no. 3, pp. 1247–1259, Jul. 2017.

[10] T. Knudsen, T. Bak, and M. Svenstrup, "Survey of wind farm control-power and fatigue optimization: Survey of wind farm control," *Wind Energy*, vol. 18, no. 8, pp. 1333–1351, Aug. 2015.

[11] H. J. Sutherland, "On the fatigue analysis of wind turbines," Sandia National Lab., Albuquerque, NM, USA; Sandia National Lab., Livermore, CA, USA, Tech Rep. SAND99-0089, Jun. 1999.

[12] *Design of Offshore Wind Turbine Structures*, DNV-OS-J101, Bærum, Norway, 2013, Art. no. 214.

[13] B. Zhang, M. Soltani, W. Hu, P. Hou, Q. Huang, and Z. Chen, "Optimized power dispatch in wind farms for power maximizing considering fatigue loads," *IEEE Trans. Sustain. Energy*, vol. 9, no. 2, pp. 862–871, Apr. 2018.

[14] T. Nguyen, A. Kashani, T. Ngo, and S. Bordas, "Deep neural network with high-order neuron for the prediction of foamed concrete strength," *Comput.-Aided Civil Infrastructure Eng.*, vol. 34, no. 4, pp. 316–332, Apr. 2019.

[15] G. Montavon, W. Samek, and K.-R. Müller, "Methods for interpreting and understanding deep neural networks," *Digit. Signal Process.*, vol. 73, pp. 1–15, Feb. 2018.

[16] A. Konak, D. W. Coit, and A. E. Smith, "Multi-objective optimization using genetic algorithms: A tutorial," *Rel. Eng. System Saf.*, vol. 91, no. 9, pp. 992–1007, Sep. 2006.

[17] J. Kennedy and R. Eberhart, "Particle swarm optimization," in *Proc. IEEE Int. Conf. Neural Netw* ., 1995, vol. 4, pp. 1942–1948.

[18] C. A. Coello Coello and M. S. Lechuga, "MOPSO: A proposal for multiple objective particle swarm optimization," in *Proc. IEEE Congr. Evol. Computation*, 2002, vol. 2, pp. 1051–1056.

[19] X. Yang and G. A. Hossein, "Bat algorithm: A novel approach for global engineering optimization," *Eng. Computations*, vol. 29, no. 5, pp. 464–483, Jan. 2012.

[20] R. Storn and K. Price, "Differential evolution–a simple and efficient heuristic for global optimization over continuous spaces," *J. Glob. Optim.*, vol. 11, no. 4, pp. 341–359, 1997.

[21] S. Mirjalili, S. M. Mirjalili, and A. Lewis, "Grey wolf optimizer," *Adv. Eng. Softw.*, vol. 69, pp. 46–61, Mar. 2014, doi: 10.1016/j.advengsoft.2013.12.007.

[22] S. Mirjalili, S. Saremi, S. M. Mirjalili, and L. dos S. Coelho, "Multi-objective grey wolf optimizer: A novel algorithm for multi-criterion optimization," *Expert Syst. Appl.*, vol. 47, pp. 106–119, Apr. 2016.

[23] J. Wang, C. Wu, and T. Niu, "A novel system for wind speed forecasting based on multi-objective optimization and echo state network," *Sustainability*, vol. 11, no. 2, Jan. 2019, Art. no. 526.

[24] Y. Yang, B. Yang, S. Wang, T. Jin, and S. Li, "An enhanced multi-objective grey wolf optimizer for service composition in cloud manufacturing," *Appl. Soft Comput.*, vol. 87, Feb. 2020, Art. no. 106003.

[25] C. Lu, L. Gao, Q. Pan, X. Li, and J. Zheng, "A multi-objective cellular grey wolf optimizer for hybrid flowshop scheduling problem considering noise pollution," *Appl. Soft Comput.*, vol. 75, pp. 728–749, Feb. 2019.

[26] M. L. Buhl, "*MCrunch User's Guide for Version 1.00*, Denver, CO, USA: Nat. Renewable Energy Lab.2008.

[27] V. Spudic, *Coordinated optimal control of wind farm active power*, Ph.D. dissertation, Univ. of Zagreb, Zagreb, Croatia, 2012.

[28] Aalborg University, "SimWindFarm toolbox," Sep. 19, 2017. Accessed: Nov. 22, 2021. [Online]. Available: https://ict-aeolus.eu/SimWindFarm/index.html
[29] J. Jonkman, S. Butterfield, W. Musial, and G. Scott, "Definition of a 5-MW reference wind turbine for offshore system development," Nat. Renewable Energy Lab., Golden, CO, USA, Tech. Rep. NREL/TP-500-38060, 947422, Feb. 2009.
[30] A. Field, *Discovering Statistics Using IBM SPSS Statistics*. London, U.K.: SAGE, 2013.
[31] W. Liu, Z. Wang, X. Liu, N. Zeng, Y. Liu, and F. E. Alsaadi, "A survey of deep neural network architectures and their applications," *Neurocomputing*, vol. 234, pp. 11–26, Apr. 2017.
[32] E. Varol Altay and B. Alatas, "Bird swarm algorithms with chaotic mapping," *Artif. Intell. Rev.*, vol. 53, no. 2, pp. 1373–1414, Feb. 2020.
[33] A. V. Tutueva, E. G. Nepomuceno, A. I. Karimov, V. S. Andreev, and D. N. Butusov, "Adaptive chaotic maps and their application to pseudo-random numbers generation," *Chaos, Solitons Fractals*, vol. 133, Apr. 2020, Art. no. 109615.
[34] F. Merahi, E. M. Berkouk, and S. Mekhilef, "New management structure of active and reactive power of a large wind farm based on multilevel converter," *Renewable Energy*, vol. 68, pp. 814–828, Aug. 2014.

Qi Yao (Member, IEEE) received the B.E. degree in automation from the School of Control and Computer Engineering, North China Electric Power University (NCEPU), Beijing, in 2014, and the Ph.D. degree in control theory and control engineering from the School of Control and Computer Engineering, NCEPU, in 2020. He is currently an Assistant Professor with Energy and Electricity Research Center, Jinan University, Guangzhou, China. His research interests include modeling, analysis and advanced control of wind turbines, and wind farms.

Bo Ma received the B.S. degree from International Energy College, Jinan University, Zhuhai, China in 2019. He is currently working toward the M.S. degree with Energy and Electricity Research Center, Jinan University. His research interests include active control and load suppression of wind farms.

Tianyang Zhao (Senior Member, IEEE) received the B.Sc., M.Sc., and Ph.D. degrees in electrical engineering from North China Electric Power University, Beijing, China, in 2011, 2013, and 2017, respectively. From July 2017 to August 2020, he was a Postdoctoral Research Fellow with Energy Research Institute, Nanyang Technological University, Singapore. He is currently an Associate Professor with Energy Electricity Research Center, International Energy College, Jinan University, Zhuhai, China. His research interests include resilience and operation research.

Yang Hu (Member, IEEE) received the B.E. degree in automation from the School of Control and Computer Engineering, North China Electric Power University (NCEPU), Beijing, China, in 2009, and the Ph.D. degree in thermal power engineering from the School of Energy, Power, and Mechanical Engineering, NCEPU, in 2015. He is currently with the School of Control and Computer Engineering. His research interests include data analysis, machine learning and optimal control of clean energy system, and integrated power system.

Fang Fang (Senior Member, IEEE) received the M.Sc. degree in control theory and engineering from North China Electric Power University (Baoding Campus), Baoding, China, in 2001, and the Ph.D. degree in thermal power engineering from North China Electric Power University, Beijing, China, in 2005.

He is currently a Professor and the Dean of the School of Control and Computer Engineering, North China Electric Power University. He has authored more than 60 high-level publications and headed more than 30 research projects or industrial projects. His current research interests include cyber-physical systems, configuration, and operation of integrated energy systems, and intelligent power generation technologies. Prof. Fang is an IET Fellow, the founding Vice Chairman of the Chinese Society for Electrical Engineering Technical Committee on Off-shore Wind Power, the Founding Vice Chairman of China Electrotechnical Society Technical Committee on Energy Intelligence, and a Council Member of IEEE IES Technical Committee on Industrial Cyber-Physical.